Heliyon 10 (2024) e35101

Contents lists available at ScienceDirect

Heliyon

journal homepage: www.cell.com/heliyon

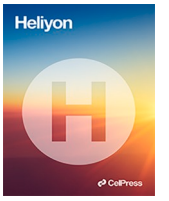

Research article

# Identification and quantification of micro–nano-plastics in polypropylene-bottled injections

Jie Wang, Lan-Gui Xie, Xian-Fu Wu, Zong-Ge Zhao, Hui-Ying Yang, Hui-Min Sun *

*National Institutes for Food and Drug Control, Beijing, 100260, PR China*

ARTICLE INFO

*Keywords:*
Polypropylene bottles
Injections
Micro–nano-plastics
Identification
Quantification

ABSTRACT

Micro–nano-plastic (MNP) particles (p) in the environment can enter the human body and pose a potential threat to human health. However, it is unknown whether these substances are present in polypropylene (PP) plastic-bottled injections, which are used as high-frequency intravenous infusions to treat diseases. Therefore, the objective of this study was to identify and quantify insoluble MNP particles in 16 batches of injectable formulations within the validity period. Primarily, ethylene–propylene copolymer or P(E–P) micro-plastic (MP) particles (2–10 μm, 216 p/mL) were identified by micro-Raman spectroscopy, and nano-particles (< 50 nm, $2.1 \times 10^4$ p/mL) similar to PP containing only carbon were detected by scanning electron microscopy–energy-dispersive X-ray spectroscopy (photoelectron). Furthermore, P(E–P) MP particles ($1 \times 10^3$ to $1 \times 10^5$ ng/L) from the injections were enriched on the GF-B filter, and PP or P(E–P) nano-plastic (NP) particles ($1 \times 10^3$ to $4 \times 10^4$ ng/L) enriched on the alumina film were detected by pyrolysis-gas chromatography/mass spectrometry. Finally, the total insoluble particles in injections were $6 \times 10^4$ to $1 \times 10^7$ p/mL (0.02–100 μm). Our findings are the first to identify and quantify MNPs in PP-bottled injections. Considering that they can enter the blood circulation, so whether cause disease remains to be investigated.

## 1. Introduction

Injection refers to a sterile liquid preparation made from raw drugs or with suitable excipients for injection into the body that can be administered sub-cutaneously, intra-dermally, intramuscularly or intravenously. Infusion, or large-volume injection, as a branch of injection, refers to a large dose of injection injected into the body via intravenous drip, with each dose being no less than 50 mL. According to the statistics of the National Health Commission of the People's Republic of China, the utilisation rate of intravenous infusion among hospitalised patients in China is approximately 80%–90 % and has remained stable [1]. Exceeding the annual consumption of 3.3 bottles (≥100 mL) per capita in developed countries, China consumed approximately 10.4 bottles in 2023. Hospital consumption is expected to maintain a 5 % increase, and it is expected to consume 15.3 billion bottles in 2024, or approximately 10.9 bottles per person.

At present, the common packaging materials used for injections mainly include medium borosilicate glass, polypropylene (PP) plastics and non-PVC co-extruded film soft bags, with PP packaging material for bottle injections accounting for the largest proportion. The technological process of large-capacity plastic bottle injections mainly includes raw material weighing, concentrated preparation (activated carbon adsorption), de-carbonisation, washing and sealing (blowing, washing and filling bottles), sterilisation, lamp

* Corresponding author.
*E-mail address:* sunhm@126.com (H.-M. Sun).

https://doi.org/10.1016/j.heliyon.2024.e35101
Received 25 June 2024; Received in revised form 9 July 2024; Accepted 23 July 2024
Available online 27 July 2024

inspection and packaging. The incomplete removal of particles during de-carbonisation, blowing and washing are potential pollution points. The PP bottle production process involves melting new PP particles or modified PP materials (obtained by dry mixing of random PP and PE elastomer) at high temperatures, injection moulding into a blank and finally ring-welding and blow moulding [2,3]. Plastic particles are easily produced during blow moulding.

The detection of insoluble particles during injection is crucial. Excessive particles can cause vascular embolism, granuloma, pulmonary hypertension and other conditions. Insoluble particles are non-metabolic impurities that are generally less than 50 μm in diameter, insoluble in water and invisible to the naked eye. According to their producing ways, these particles can be divided into endogenous and exogenous types. The former category refers to residual impurities or insoluble inorganic salts in the raw and auxiliary materials introduced during injection and other injection processes, glass debris or silicate particles introduced into the glass bottle container, plastic particles introduced through the penetration of plastic bottle membranes, desquamated particles from direct contact with the drug packaging material and particles caused by improper transportation or storage [4]. In contrast, the latter category refers to particles shed from equipment; particles introduced by the non-standard operation of workers, environmental dust, hair and microorganisms; and particles introduced during clinical use [5]. Because the diameter of human capillary vessels ranges from 4 to 9 μm [6], particles larger than 10 μm easily block blood vessels, resulting in local embolism and necrosis [7]. The pharmacopoeias of each country specify the limits of particles in drugs containing particles larger than 10 μm. For volumes of 100 mL or more, the limit was set to ≤12 particles/mL, whereas for volumes less than 100 mL, the limit was set to ≤3000 particles/package [8–10].

Micro–nano-plastic (MNP) particles, as a type of insoluble particles in the injections, have been detected in 500-mL PP bottle injections irradiated with UV340 nm for 6 weeks (20–50 μm, 0.105 mg) [11] but not reported in the injections packaged with the same material without any treatment within the validity period. Although particles smaller than 10 μm are not limited by the pharmacopoeia, they can pass through blood vessels and enter tissues of the body, such as the liver and spleen [12]. Larger MNP particles can cause cellular damage. For example, PP micro-plastic (MP) particles (particularly those sized at 8 μm and 24 μg, 0.66 μm and 87.5–175 μg) promote oxidative stress and inflammation, causing colon apoptosis and lung injury in mice [13,14]. Nevertheless, particles smaller than 500 nm can be internalised into cells, causing chromosomal aberrations and organelle damage. Thus, they are risk factors for vascular malformations, liver dysfunction and pathological pregnancy [15–18]. In contrast to MNP particles in food, which are ingested by the human body through the mouth and can enter organs such as the gastrointestinal tract, MNP particles inhaled from clothes can enter the lungs. Injections can be directly delivered into the bloodstream, reaching organs such as the heart, lungs and liver. Nano-particles (≤293 nm) can even penetrate the blood–brain barrier [19] and access the brain, thereby affecting the entire body. Finally, because of their large specific surface area, plastic particles can strongly adsorb antibiotics, oestradiol, albumin and globulin, which may affect their activity and dosage [20–23].

Insoluble MNP particles in plastic-bottled (bag) injections may be produced during the bottle blowing and washing, filling and sealing processes and due to factors such as the compatibility of the drug and the packaging material, transportation conditions and improper storage. These particles were detected at a concentration of 210 μg/L in the injections that underwent simulated sunlight irradiation at UV-340 nm for the accelerated ageing experiments but not in injections without treatment. Based on people using intravenous infusion to treat diseases frequently, MNP particles can directly enter organs of the body through the blood, and some nano-plastic (NP) particles can even enter cells, causing body damage. Therefore, given the potential threat to human health caused by insoluble MNP particles, there is an urgent need to develop accurate methods to identify and quantify MNP particles in injections. In this study (Fig. 1), micro-Raman (μRaman) spectroscopy and scanning electron microscopy (SEM) were used to identify MNP particles in commonly used injections, and pyrolysis-gas chromatography/mass spectrometry (Py-GC/MS) was used for qualitative review and quantitative analysis. We obtained the size and concentration data of MNP particles in injections within the validity period for the first time, laying a good foundation for the next study of their toxicological effects on mice and zebrafish. In addition, this study sets the stage for the final investigation of the potentially harmful effects on human organs.

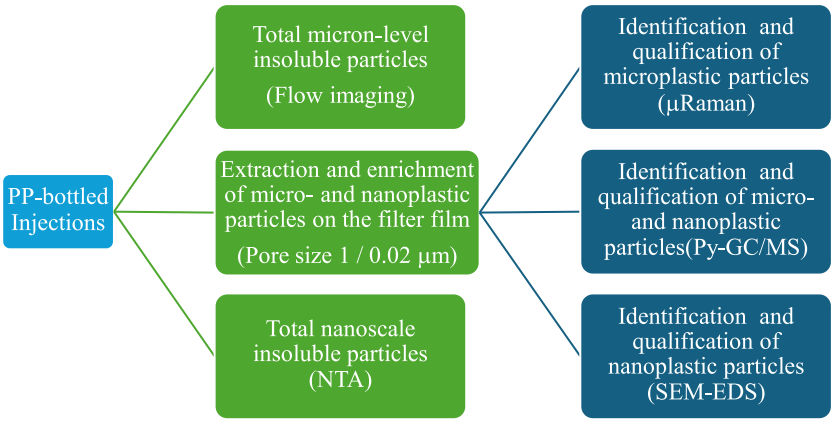


**Fig. 1.** Overview of the study protocol. Material specification and technologies used in the study were noted in bracket. The research was performed from left to right.

## 2. Materials and methods

### 2.1. Materials

Disposable syringes (1 mL) were purchased from the Shandong WEGO Group. Disposable aseptic tape filter suction heads were obtained from Eppendorf (Cat. No. 0030015258). Sterile transparent round concave-bottom 96-well plates were purchased from Greiner (Cat. No. 650101). PP micro-powder was from Zancheng (Tianjin) Technology Co., Ltd. (Code: BR06754). PP nano-particles were obtained from Hubei Xinyuhong Bio-medical Technology Co., Ltd. (Cat. No. PP-0100N). The glass filter device was purchased from Shandong Feida Glass Instrument Co., Ltd. (Cat. No. FD-V-01250). Glass fibre (pore size 1 μm, 1821-047) and alumina filter membrane (pore size 20 nm, 6809-6002) were purchased from Waterman. Sixteen batches of injections were commercially purchased, including 2 batches of glucose, 1 batch of sodium bicarbonate, 1 batch of metronidazole sodium chloride and 12 batches of sodium chloride (Table 1).

### 2.2. Methods

#### 2.2.1. Identification and quantification of micro-plastic particles in injections by μRaman

1. Sample preparation

Under a vertical super-clean bench (Protect-1FD, Thermo, USA), the aseptic alumina filter membrane (20 nm) was clamped to the clean glass filter device, and 10 injection bottles were poured (a total of 1 L) into the filter cup, followed by vacuum pumping (0.2 MPa) and filtering. Finally, the filter film was transferred to a clean glass dish, air-dried naturally and sealed with a sealing film. During the processing described above, an alumina filter membrane without any treatment was used as a negative control and was simultaneously tested by μRaman spectroscopy using the sample membrane described above (DXR 2Xi, Thermo Scientific, USA).

2. Instrument condition

The detailed parameters for conducting μRaman spectroscopy were as follows: 100 × objective, 532-nm laser wavelength, 10-mW laser power, 0.04 s exposure time, 1000 exposures and a spectrum recording interval of 200–3400 $cm^{-1}$. The polymer spectrum was entered into the library [24], and its type was determined based on its similarity to the standard material (≥60 %).

#### 2.2.2. Identification and quantification by Py-GC/MS

1. Sample extraction and enrichment

Sample preparation on the super-clean bench. First, the glass fibre film (GF-B, aperture 1 μm) was heated in a muffle furnace at 500 °C for 1 h to remove impurities. Second, the GF-B fibre film was fixed on the glass pumping filter device, and 10 injection bottles (100 mL/bottle) were normally added to the filter cup. The filtered solution was then placed in a clean glass triangular bottle. Third, the filter film was transferred to a clean glass dish using a clean stainless steel tweezer and sealed after natural air drying before testing. Fourthly, sterile water for injection (1 L) was treated in the same process as in the first and second steps but with a clean alumina film. In addition, the filter membrane without any treatment in the ultra-clean table during the entire process, the blank GF, $Al_2O_3$, the filtered water membrane, the filtered sample GF-B membrane and the $Al_2O_3$ membrane were each cut and placed in the pyrolysis cup

**Table 1**
Detailed information of 16 batches of injections.

| Manufacturers | Batch number | Drugs (100 mL/bottle) |
|---|---|---|
| A | A01 | 5 % $NaHCO_3$ |
| B | B01 | 5 % Glucose |
| C | C01 | 5 % Glucose |
| E | E01 | 0.9 % NaCl |
| F | F01 | 0.9 % NaCl |
| | F02 | |
| G | G01 | 0.9 % NaCl |
| H | H01 | 0.9 % NaCl |
| I | I01 | 0.9 % NaCl |
| J | J01 | 0.9 % NaCl |
| K | K01 | 0.9 % NaCl |
| L | L01 | 0.9 % NaCl |
| M | M01 | 0.9 % NaCl |
| N | N01 | 0.9 % NaCl |
| O | O01 | 0.9 % NaCl |
| P | P01 | 0.9 % NaCl-0.2%metronidazole |

for analysis, along with the blank pyrolysis cup. Each sample was analysed three times (approximately 5 mg GF and 3 mg alumina membrane to be analysed per piece, accounting for 1/6 of the whole film). Finally, the obtained spectra were added to the polymer spectrum library, and the compound types were identified using the F-search software.

2. Instrument condition

Analysis was performed using the multi-shot pyrolysis unit EGA/PY-3030D (Frontier Laboratories, Japan) in 'double shot' mode. The detailed parameters were as follows. First, the samples were heated from an initial temperature of 100 °C–300 °C at a rate of 50 °C/min in the pyrolyser furnace and held for 1 min for thermal desorption analysis. The GC/MS system (GC–2030, GCMS-QP2020 NX, Shimadzu, Japan) was equipped with an SH-Rxi-5Sil MS column (30 m × 0.25 mm × 0.25 μm, Frontier Laboratories, USA). Measurements were performed in full-scan and split modes (1:100 split ratio). The compounds were trapped in the GC column after pyrolysis. Second, the column was programmed from an initial temperature of 60 °C (2 min) to 230 °C at a rate of 20 °C/min, followed by a ramp of 50 °C/min to 320 °C (12 min), resulting in a total run time of 24.3 min. Third, after the thermal desorption procedure, the pyrolysis furnace was heated to 600 °C and kept for 20 s for the next measurement (pyrolysis). Finally, the column was programmed from 60 °C (2 min) to 320 °C at a rate of 40 °C/min and maintained for 20 min, resulting in a total run time of 28.5 min. The temperatures of the injected port, interface and ESI were set to 300 °C, 280 °C and 230 °C, respectively.

3. Standard curve and recovery experiment

Standard curve. Initially, 2 mg of the PP particles was mixed thoroughly with 20 mL of ethanol using a stirrer. Next, 4, 20, 100, 200, 500 and 2500 μL of the particulate suspension were absorbed and re-mixed in 20 mL of ethanol. The filter membrane containing the standard samples was prepared according to the extraction step described in Section 2.2.1. Finally, half of the filter membrane was placed in the pyrolysis cup for simultaneous analysis with the above samples, and the peak area of the characteristic ion ($m/z = 126$) at the target peak was calculated [25]. Cautions: the target peak areas at the two lowest concentrations were used to determine minimum detection and quantification limits according to the signal-to-noise (S/N) ratio [26]. The amount of PP in the spiked sample was set according to the lowest, average and highest contents of MNPs during injection, and the recovery rate of the sample were analysed. First, 0.02, 0.2 and 2 mL of the suspension were absorbed and diluted to 20 mL with ethanol. The GF filter membrane containing the labelled sample was prepared according to the extraction filtration steps described in Section 2.2.1. In the end, they were placed into a pyrolysis cup after cutting, along with 1, 10 and 100 μg of PP particles obtained by normal weighing, for thermal cracking analysis (Py-GC/MS). Excel® was used to draw the standard curve.

### *2.3. Quantification of total micro-metre-level insoluble particles using Flowcam 8100*

#### *2.3.1. Sample preparation*

After washing the flow imaging system Flowcam 8100 (Yokogawa Fluid Imaging Technologies, USA) with sterile water for injection, the number of micro-particles in 10 water bottles was measured, and the average was recorded as negative control 1 (NG1). Before measuring the number of particles in the water, 10 disposable syringes were used to transfer the same amount of water to the instrument, and the average was calculated as the sum of the number of particles in the water and the syringe. The number of particles in the water was subtracted, and the number of particles in the syringe was recorded as negative control 2 (NG2). Finally, insoluble particles in 16 batches of injections were analysed sequentially.

#### *2.3.2. Instrument condition*

First, the injections were shaken well before each measurement. Then, a disposable sterile syringe was used to draw the liquid from the bottle and dispense it into the concave-bottom 96-well plate, with 250 μL added to each of the three holes (Priming: machine prime; Flow cell type: FC80FV). Second, the sample was measured in each hole, and the system was flushed twice with an equal volume of water. Finally, the number of micro-particles in each injection was determined by subtracting the quantity determined in the water and syringe from the measured data. The flow rate, autoimage rate, sampling efficiency, and segmentation threshold (dark/light) were set for 0.15 mL/min, 10 frames/s, approximately 70 %, and 15/15, respectively.

### *2.4. Identification and quantification of NP particles in injections*

#### *2.4.1. Identification and quantification by SEM-EDS*

1. Sample preparation

In the vertical super-clean bench, the GF-B filter membrane (1 μm) was burned in a muffle furnace (500 °C, 1 h) and then fixed on a clean glass filter. After the injections (10 × 100 mL) were pumped using a vacuum pump, the filtrate was poured into a clean glass filter with an aseptic alumina film (20 nm) and pumped again. The alumina filter membrane was then transferred to a clean glass dish using a clean stainless steel tweezer and closed for analysis after natural air drying. Subsequently, 10-mg nano-particles were mixed with water before pumping and filtering manner as above to prepare positive control products, which were then closed after natural air drying. Meanwhile, the alumina filter membrane without any treatment was placed on the ultra-clean table to serve as the negative

control. These three conditions were simultaneously analysed using SEM-EDS (ProX, PhenomWorld, China).

2. Instrument condition

Single-particle imaging was performed at an accelerating voltage of 15 kV in backscattered electron mode under a vacuum of 0.1 Pa, with a refresh frequency of 6.3 Hz and exposure time of 24 s. EDS spectrum scanning was performed in the point-scanning mode.

*2.4.2. Identification and quantification by Py-GC/MS*

In the vertical super-clean bench, the solution filtered through the GF-B membrane (Section 2.2.2) was poured into the clean glass filter device containing the fixed alumina film. Step 1 of Section 2.2.2 was repeated. The acquired filter film enriched with insoluble nano-particles was analysed by Py-GC/MS, along with the samples described in Section 2.2.2.

Quantification was performed according to the standard curve constructed in the step 3 of Section 2.2.2, and the recovery rate was determined simultaneously.

*2.5. Quantification of the total nano-scale insoluble particles by nanoparticle tracking analyzer*

*2.5.1. Sample preparation*

First, the instrument (Nano-Sight, Malvern Panalytical, German) was washed with sterile water for injection and transferred using a disposable syringe. Next, after the flow cell was cleaned by manual injection of 0.5 mL of the solution with a syringe containing 1 mL of the liquid, image calibration was performed with the largest proportion of particles present in the liquid. Then, the syringe containing liquid was fixed to the injection device, and the number of insoluble nano-particles in the water and 16 batches of injections were determined by an automatic injection mode.

*2.5.2. Instrument condition*

The test process was as follows. (1) The system was flushed with the sample liquid for 5 s at a pump speed of 1000. (2) The system was balanced for 10 s using the sample liquid at a pump speed of 50. (3) Image capture was performed for 60 s, and after 1-s delay, the measurement was repeated for rounds. (4) After each measurement was completed, the results were automatically analysed to obtain the particle size distribution and concentration data. Each sample was analysed three times.

*2.6. Quality control*

Throughout the experiment, sterile water for injection was used as a programmed blank sample, after each cleaning of the experimental equipment such as the extraction filter device, it was pumped to the membrane with the same volume. When no MNP particles were detected in the water filter film, the glass pumping filter device could be used for the particle enrichment of next batch of injection. Secondly, each enrichment experiment was completed under the vertical flow clean bench, and a blank filter film was placed under the whole experiment process as a blank control. After filtration, the film was left to dry in a clean glass dish, and the blank film

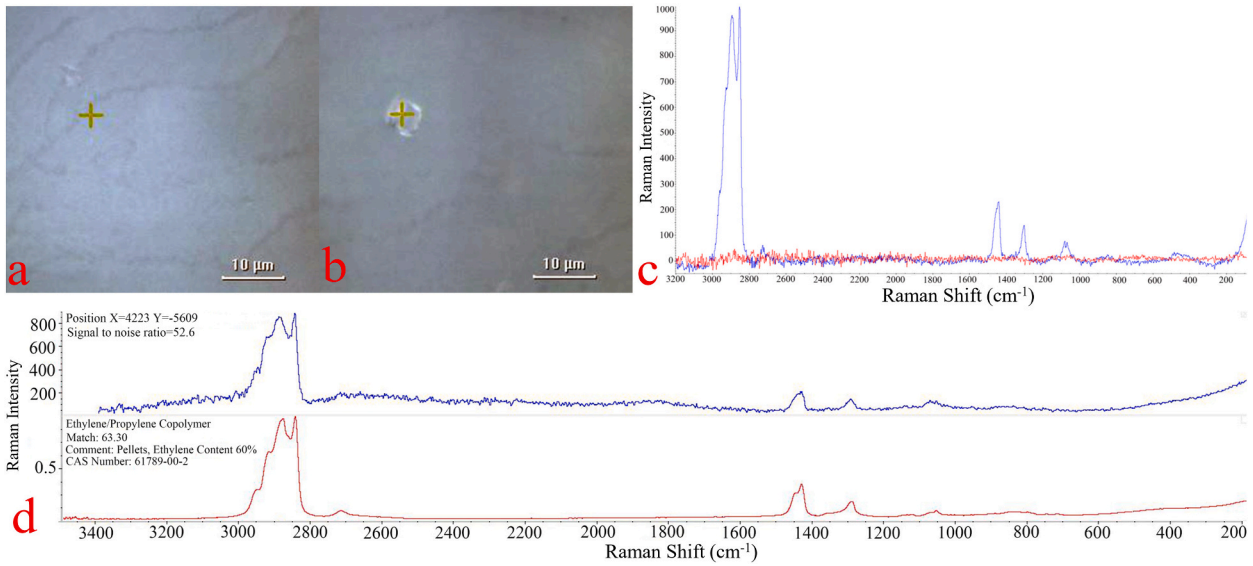


**Fig. 2.** μRaman identification of microplastic particles in injections. (a) Blank control. (b) The polymer particles from an injection of manufacturer F02 enriched on the Al2O3 filter film. (c) The spectrum of the blank control (red) and polymer particle (blue). (d) The material information of polymer particle matched to spectrum library

was also left to dry in another glass dish for comparison. Before each sample detection, the same Py-GC/MS procedure was used to detect the blank lysis cup until no MNPs appeared 3 times. The whole process of enrichment and analysis strictly reduces and controls the background pollution.

### 2.7. Statistical analysis

All data were analysed mainly by the software configured for each instrument and GraphPad Prism 5.0 and are expressed as the means ± standard deviation. Statistical difference was evaluated with Student's *t*-test, with differences considered significant at $P < 0.05$ as indicated in figure legends.

## 3. Results

### 3.1. Size, quantity and concentration of MP particles in PP plastic-bottled injections

The particles in liquids enriched on the $Al_2O_3$ filter membrane were analysed by μRaman spectroscopy. No polymer particles were observed on the control membrane, whereas polymer particles with diameters close to 5 μm were observed on the particle membrane after the enriched F01 injection (0.9 % NaCl) as representative of all injections (Fig. 2a–c). Among the 16 injection batches, 15 batches of MP particles were detected (Fig. S1), and all samples were between 2 and 10 μm. In Fig. 2c, the peak observed at 2800–3000 $cm^{-1}$ represents the stretching vibration of the C–H bond of CH3 and CH2, the peak at 1448 $cm^{-1}$ represents the C–H interatomic flexural vibration of PP, the peak at 1290 $cm^{-1}$ represents the C–H interatomic rocking vibration peak of PE, the peak at 1125 $cm^{-1}$ represents the symmetric stretching vibration peak between C atoms of PE, the peak at 1060 $cm^{-1}$ represents the asymmetric stretching vibration peak between C atoms of PE, the peak at 973 $cm^{-1}$ represents the asymmetric vibration peak between C atoms of PP and the peak at 842 $cm^{-1}$ represents the C–H interatomic wobble vibration peak of PP. Therefore, a fragment was identified as P(E–P) by spectroscopic

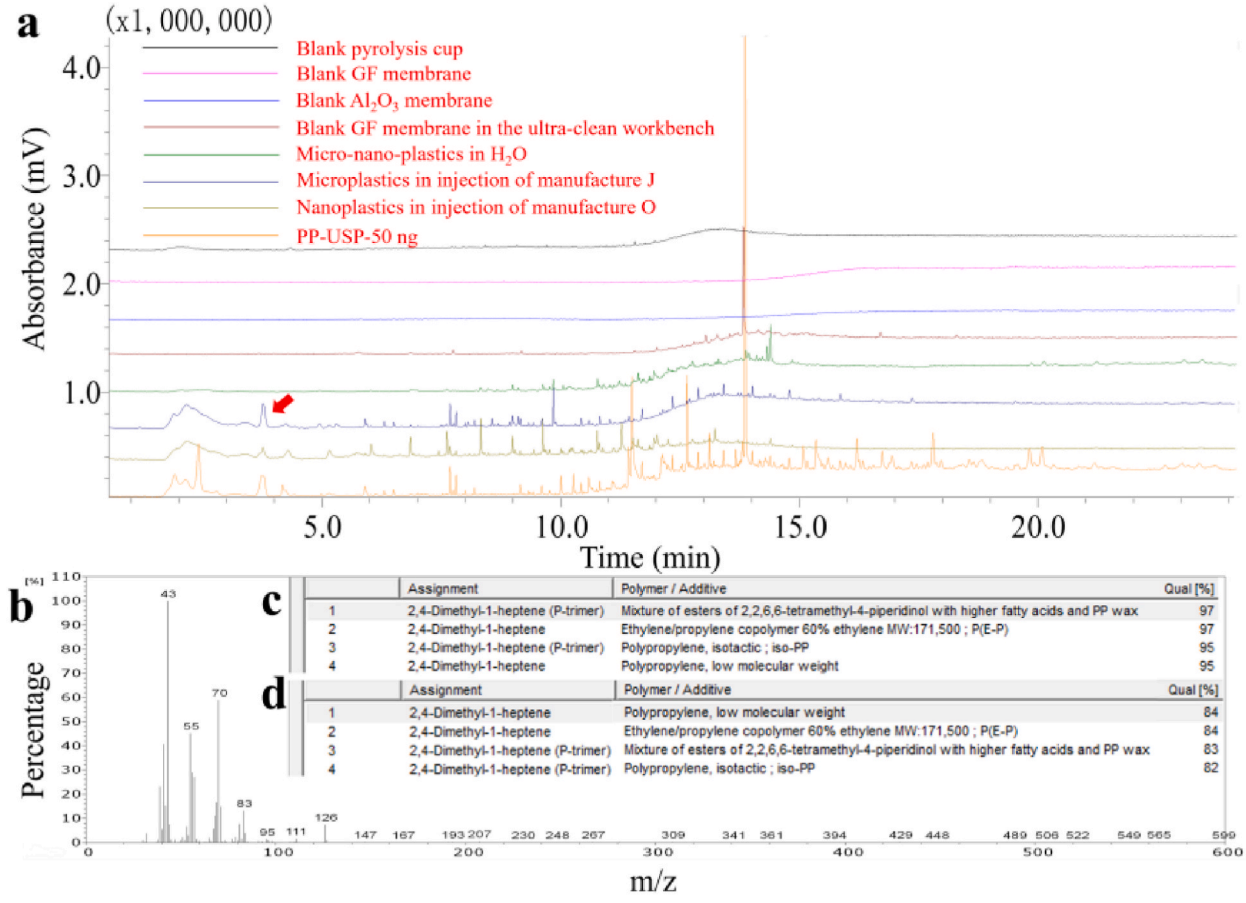


**Fig. 3.** Py-GC/MS identification of the MNP insoluble particles in injections. (a) The particle spectrums of the negative control, injection, and positive control were analysed by GC. (b) The MS information at the target peak location (red arrow). (c, d) The material matching information at the target peak location was searched in the spectrum library by F-Search software which indicated the MP and NP insoluble particles. (For interpretation of the references to colour in this figure legend, the reader is referred to the Web version of this article.)

search and comparison with the polymer library (Fig. 2d). There were 2.16 × $10^5$ MPs per litre of injection, equivalent to approximately 216 MP/mL.

The particles and fragments enriched on the GF-B membrane (aperture 1 μm) were analysed using Py-GC/MS. The blank pyrolysis cup, GF-B and $Al_2O_3$ membrane, filter membrane in the benchtop and film enriched with water particles were not detected, whereas a characteristic peak appeared at 3.5 min of particle analysis (Fig. 3a, dark blue line) on the membrane of the enriched injection was the same as that of PPs included in the United States Pharmacopoeia (USP). The characteristic peak component containing ions with *m/z* values of 43, 55, 70, 83 and 126 (Fig. 3b). After comparing the spectra of the substances composed of the above ions with those in the polymer spectrum library, the P(E–P) copolymer with a maximum similarity of 97 % was identified (Fig. 3c). The remaining samples were identified as various forms of PP with a similarity of 95 %. In summary, the presence of P(E–P) and other MNPs in the injections was determined using Py-GC/MS.

Because of the low frequency of *m/z* 126 in the ionic fragments of other compounds, and its strong specificity among the five fragment ions in PP [25], it was selected as a quantitative ion (Fig. 4a). Different concentrations of PP particles enriched on the filter membrane were analysed using Py-GC/MS. The *m/z* 126 peak area at 3.5 min was statistically analysed to obtain a standard curve (Fig. 4b). According to the ICH methodology validation Q2(R1), the minimum detection limit was 2 ng for 3 S/N, and the limit of quantification (LOQ) was 10 ng for 10 S/N (Fig. S2). After quantification using the standard curve, no MPs were detected in the injections from manufacturer E (0.9 % NaCl). Among the injections in which MPs were detected, the N injection (0.9 % NaCl) had the lowest MP concentration (1463.7 ng/L), and the J injection (0.9 % NaCl) had the highest concentration (43,514.7 ng/L). The average and median concentrations were 10,627.3 and 6626.3 ng/L, respectively (slash line box in Fig. 4c). Remarkably, insoluble MP particles were detected in the two batches of injections from manufacturer F (0.9 % NaCl). In addition, the peak area of fragment ion *m/z* 126 at the target position of the spectrum was obtained through Py-GC/MS analysis of PP particles in enriched spiked samples and PP particles directly weighed at the same time (Table 2). The recovery rate was calculated by dividing the ion *m/z* 126 peak area by the former and then multiplying by 100 %. The recovery rates for low, medium and high concentrations were 15.6 %, 22.7 % and 31.6 %, respectively.

### 3.2. Quantity and size distribution of the total micro-metre-level insoluble particles (p) in injections

Analysis using the Flowcam 8100 flow particle imaging system revealed the presence of particles in various forms, such as silicone

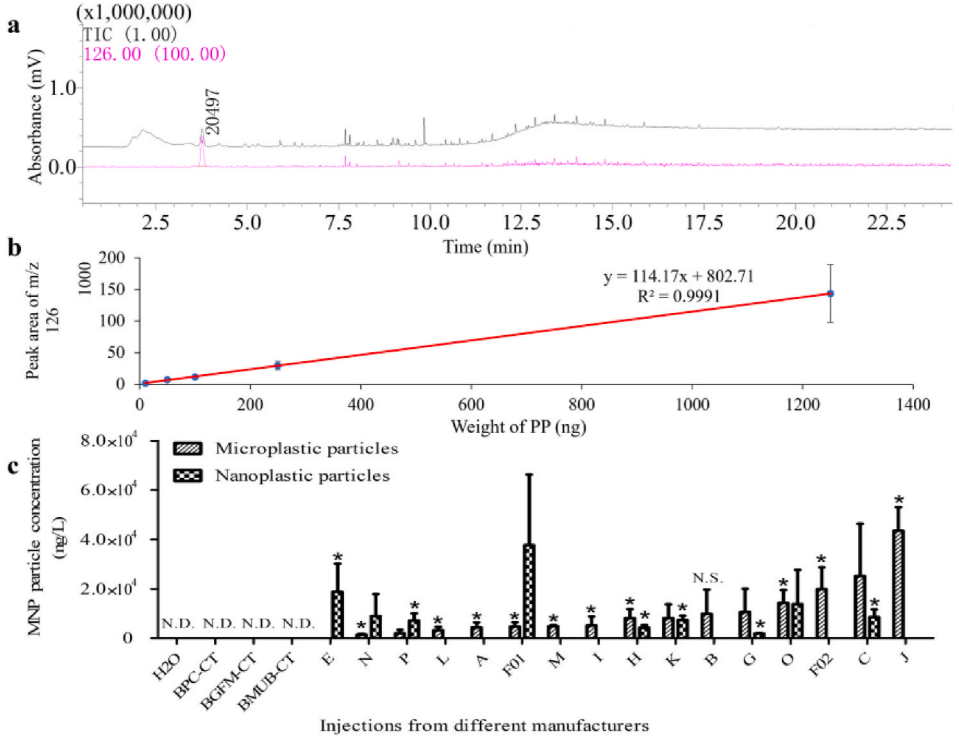


**Fig. 4.** Py-GC/MS quantitative analysis of MNP particles in injections. (a) The TIC and fragment ion m/z=126 spectrum of insoluble particles in the membrane enriched from injection. (b) The standard curve was formed from the peak area of the corresponding ion m/z=126 at the target position of the spectrum for 10 ng, 50 ng, and 250 ng standard PP particles, respectively. (c) The amount of MNP insoluble particles was calculated by the standard curve in the injections. N.D., not detected; BPC-CT, blank pyrolysis cup-control; BGFM, blank GF membrane; BUMB, blank GF membrane under benchtop; N.S., no significance. Values are presented as the mean ± standard error of three replicate samples. *P < 0.05 indicates significant differences when compared to the control.

**Table 2**
Recovery analysis of extraction and enrichment samples by Py-GC/MS (ratio of *m/z* 126 peak area).

| Spiked samples (Split ratio, 1:100) | Spiked samples enriched in filtered film | | | Weighted PP samples | | | Recovery |
|---|---|---|---|---|---|---|---|
| | $1_{st}$ | $2_{nd}$ | $3_{rd}$ | $1_{st}$ | $2_{nd}$ | $3_{rd}$ | |
| 1 μg (10 ng) | 578 | 564 | 643 | 3586 | 4660 | 3189 | 15.6 % |
| 10 μg (100 ng) | 34078 | 68031 | 28582 | 95421 | 237254 | 243926 | 22.7 % |
| 100 μg (1 μg) | 680314 | 688877 | 645207 | 2,014,806 | 1,955,303 | 2,404,572 | 31.6 % |

oil, protein analogues, metal or carbon particle analogues and MP debris analogues (Fig. 5Aa–Ad). In negative control 1, the concentration in sterile water for injection was 126–547 p/mL, with an average of 350 p/mL and a median of 400 p/mL. The size distribution was as follows: 1–2 μm with a proportion of 41.47 %, 2–10 μm with 56.41 % and more than 10 μm with 2.12 %. In negative control 2, the particle quantity in the syringes ranged from 22 to $9.9 \times 10^4$, with an average of 12000 particles and a median of 5127 particles. The size distribution was as follows: 1–2 μm with a ratio of 30.88 %, 2–10 μm with 68.33 % and more than 10 μm with 0.79 %. After background deduction, among the 16 batches of injections, the lowest concentration was 3378 p/mL for the E injection (0.9 % NaCl), and the highest concentration was 46,500 p/mL for the J injection (0.9 % NaCl). The average and median concentrations were 13,217 and 10,842 p/mL, respectively (Fig. 5B).

### *3.3. Size, quantity and concentration of NP particles in PP plastic-bottled injections*

The untreated $Al_2O_3$ film, the enriched 100 nm PP particle film, and the enriched particle film after injection were compared and analysed using SEM-EDS. In the untreated film, only the Al and O elements with atomic (2:3) and mass (9:8) ratios corresponding to those of the film and the sprayed gold elements were found (Fig. 6a). However, in addition to the correct proportions of Al and O and sprayed gold elements in the film, C element with 1.09 % of the mass concentration was detected in the standard PP particles (Fig. 6b). Approximately 48-nm polymer particles were captured in the enriched sample film, with approximately $2.1 \times 10^7$ polymer particles/L ($2.1 \times 10^4$ polymer particles/mL). Their C element mass ratio was 0.53 % (Fig. 6c). In summary, apart from the Al and O elements that comprise the filter film, and sprayed Au elements, the particle size and the mass proportion of the C element were positively correlated. Therefore, it is presumed that the injection contains NP fragments that below 50 nm.

Py-GC/MS analysis of the insoluble NP particles and fragments enriched on the alumina membrane (20 nm) revealed that no such particles were found in the blank lysis cup, $Al_2O_3$ membrane, ultra-clean platform filter membrane and filter water film. However, the

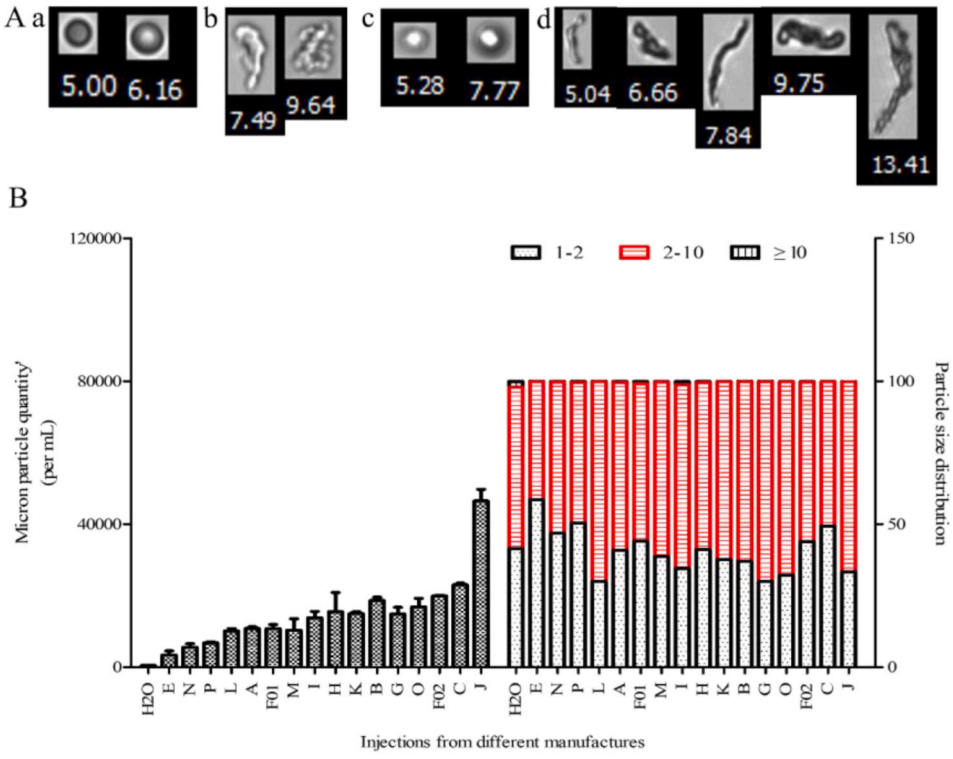


**Fig. 5.** Flowcam determination of quantity, and size distribution of micrometer-level insoluble particles. (A) Particles of various shapes were photographed with a 10x objective lens (unit: $\mu$m). (B) Concentration (left) and size distribution (right) of micron-sized particles in the injections.

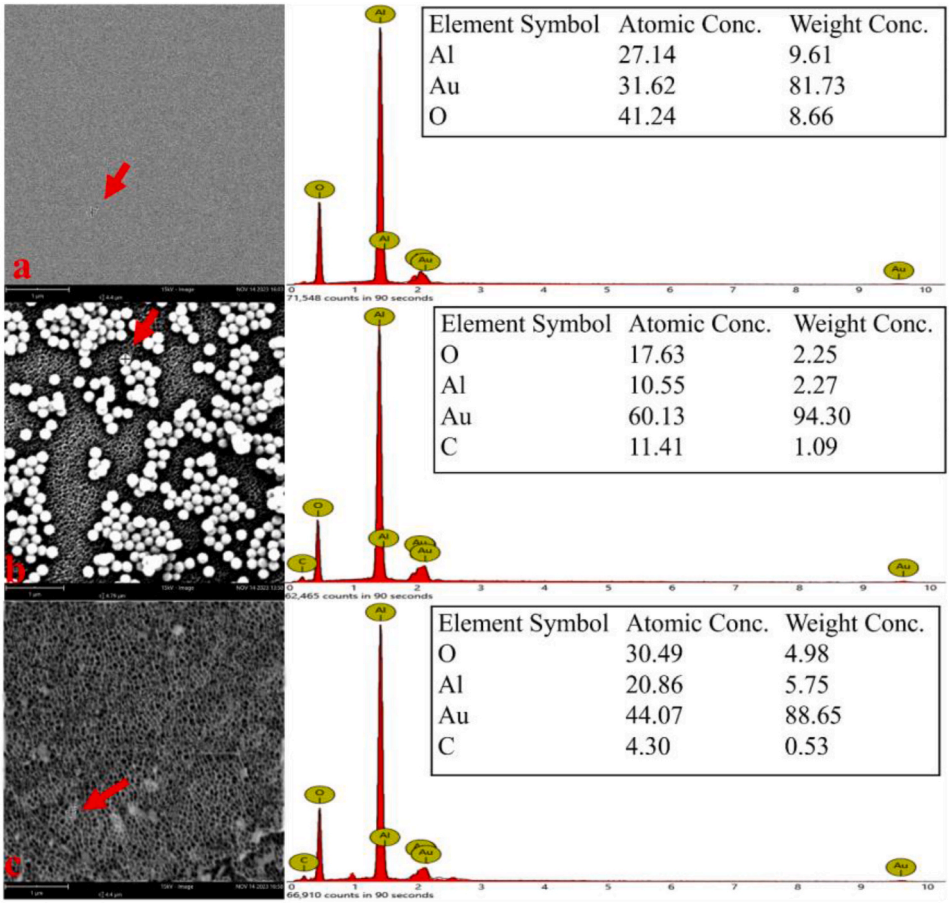


**Fig. 6.** SEM-EDS identification of nano plastic particles in insoluble particles of injections. The image and element information of point (a) and standard PP particles (b) in the blank and enriched particles Al2O3 membranes respectively. (c) The image and element information of particles which similar to PP on the membrane enriched from the injection of manufacturer F.

characteristic peak observed at 3.5 min of particle analysis on the membrane of the enriched injection was the same as that of PP included in the USP (Fig. 3a, light green line, manufacturer O, 0.9 % NaCl). A spectral library search of the substances composed of the five major ions contained in the characteristic peak component (Fig. 3b) was performed. PP or P(E–P) was identified with a maximum similarity of 84 % (Fig. 3d). In conclusion, insoluble particles such as P(E–P) or PP exist in the injection within the validity period.

According to the standard curve shown in Fig. 3b, in contrast to A (5 % $NaHCO_3$), B (5 % Glucose), F02 (0.9 % NaCl), I (0.9 % NaCl), J (0.9 % NaCl), L (0.9 % NaCl), M (0.9 % NaCl), in which no NPs were detected, manufacturer G injection (0.9 % NaCl) had the lowest concentration (1852.59 ng/L) and F01 had the highest concentration (37,612.7 ng/L). The average and median concentrations were 6613.16 and 5056.32 ng/L, respectively (black and white columns in Fig. 4c).

Through the detection of NTA (Fig. 7a), it was found that the particle size of the control of sterile water for injection was 80–400 nm, and the average concentration was $2.92 \times 10^6$ p/mL. Nevertheless, the particle size of 16 batches of injections ranged from 20 to 900 nm, except for A, B, F02, I, J, L and M. Particles below 50 nm in size were distributed in other manufacturers (Fig. 7b). Among the 16 batches of injections, the injection of manufacturer N (0.9 % NaCl) had the lowest concentration ($6.24 \times 10^4$ p/mL), and P (0.9 % NaCl–0.2 % metronidazole) had the highest concentration ($9.15 \times 10^6$ p/mL). The average and median concentrations were $1.91 \times 10^6$ and $6.76 \times 10^5$ p/mL, respectively (Fig. 7c).

## 4. Discussion

This study identified its presence of MNP particles in chemical injections for the first time and measured their concentrations and sizes. Results from μRaman analysis of MP particles indicated that the number of insoluble micro-particles ranged from $3 \times 10^3$ to $5 \times 10^4$ p/mL and their size distribution in terms of quantity was as follows: 2–10 > 1–2 > 10 μm. Py-GC/MS analysis of 16 batches of injections suggested that the size of insoluble MP particles mainly ranged from 2 to 10 μm, and the concentrations ranging from $1 \times 10^3$ to $1 \times 10^5$ ng/L were detected in injections from 16 manufacturers. In summary, in this section, considering insoluble particles of 2–10 μm as an MP marker, MPs can be detected using the current Py-GC/MS method when the concentration of the marker exceeds 1000 p/

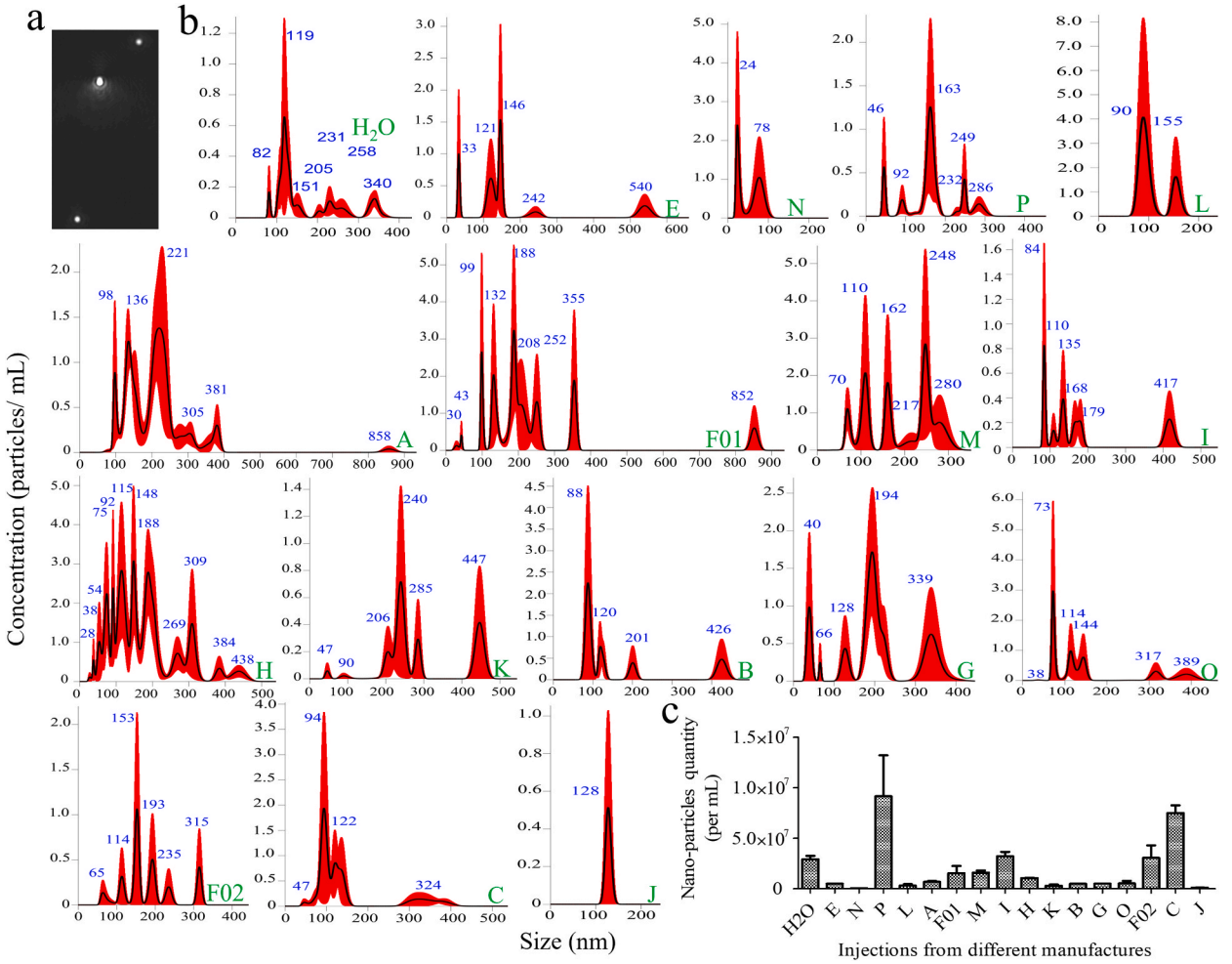


**Fig. 7.** NTA determination of concentration and size distribution of insoluble nano-particles. (a) The particles were captured by NTA. (b) The size distribution of particles in injections and sterile water for injection. Green letters indicated various manufacturers of injections. (c) The total insoluble nano-particles concentration in sterile water for injection and 16 batches of injections were analysed by GraphPad Prism 5.0. (For interpretation of the references to colour in this figure legend, the reader is referred to the Web version of this article.)

mL. In combination with the SEM-EDS results, which determined the number of insoluble nano-particles to range from $1 \times 10^5$ to $1 \times 10^7$ per millilitre, with a size distribution of 20–900 nm, and Py-GC/MS data, it was found that the size of NPs in the injections was mainly distributed below 50 nm. Nine batches were detected with concentrations ranging from $1 \times 10^3$ to $4 \times 10^4$ ng/L. Together, these data represent the appearance and size of MNP particles in injections show the quantity and concentration, and let people have the comprehensive knowledge of its existence.

### *4.1. Evaluation of MNP particle identification by μRaman and SEM-EDS*

In view of the fact that the actual spatial resolution of is 1 μm, which is not interfered by nanoparticles, and the low background Raman signal of alumina filter with pore size of 0.02 μm [27], it was directly used to enrich the particles in the injection and then identify the presence of microplastics without damage. Due to the weak Raman signal defect, the laser intensity must reach 10 mW for the actual determination. Since the compatibility of liquid medicine and plastic bottles may induce the emergence of MNP particles [5]. The copolymers of ethylene-propylene with irregular shapes and smooth surfaces were found for the first time in the chemical injection through μRaman spectroscopy (Fig. 2 and Fig. S1), with sizes ranging from 2 to 10 μm and approximately 216 p/mL. These sizes are slightly smaller than MPs detected in beverages such as water (10–1000 μm), milk (5–20 μm) and beer (100 μm–5 mm), whereas the concentrations were slightly higher than those found in water (20–120 p/L), milk (2–10 p/mL) and beer (20–80 p/mL) [28–31] and lower than that released by polyester (PL) clothing ($2.8 \times 10^3$ p/g) [32]. In addition, it may not be detected due to the small contact area of liquid with bottles in 500 mL injection [11], based on nearly 4 times contact area than before 10 bottles of 100 mL injections were used to measure together, and the measured MNP content ruled out the negative result ultimately.

In consideration of the limitation of μRaman resolution, the nanoparticles can only be identified by SEM-EDS just as identifying the

types of marine NPs via SEM [33], and the injection is first filtered through a 1 μm GF-B membrane and then further collected by an alumina membrane to eliminate the interference of micron particles. Furthermore, in order to make up for the defect that EDS cannot detect H element in polymers [34], particles of 100 nm PP were introduced as a positive control in this study to assist in identifying plastic particles according to carbon content and particle size. SEM - EDS was used to identify particles or fragments present in the injection with a similar proportion of elements as PP particles for the first time (Fig. 6). These NP particles were found at sizes of $<50$ nm, with an estimated concentration of $2.1 \times 10^4$ p/mL, which is higher than that detected in bottled water (216 p/mL) [35] and lower than that of NPs released in PL clothing ($3.3 \times 10^{11}$ p/g) [32]. Because MNPs not only appeared during the processes of filling and sealing but also resulted from the degradation of the plastic-bottled water [36,37], they may be generated in the same manner in PP-bottled injections.

In conclusion, the two methods complement each other, which are used to characterize the appearance and size of MNP and semi-quantitative particle numbers in the injections.

### 4.2. Evaluation of the total insoluble particles' quantification using Flowcam 8100 and NTA

Following the micro-flow imaging method for the determination of insoluble particles in pharmaceutical products as prescribed in section <1788.3> of the USP, the Flowcam 8100 was used to evaluate the number of insoluble micro-particles in injections ($\geq$100 mL) for the first time. The concentration ranged from $3 \times 10^3$ to $5 \times 10^4$ p/mL between 1 and 100 μm (Fig. 5). Because no significant difference was observed between Flowcam and microscope determinations of dinoflagellate number [38], our results are scientifically reliable and accurate. In addition, the limit of the number of micro-particles $\geq$10 and 25 μm in 100-mL filling-volume injections is consistent with those indicated in the pharmacopoeias of all countries, such as USP43–NF38, European Pharmacopoeia 10.0 and Chinese Pharmacopoeia 2020, with limits set as $\leq$12 and 2 particles/mL. The data of corresponding particles in 16 batches of chemical injections tested in this study all meet the requirements of the pharmacopoeias. However, the number of particles from 1 to 10 μm that were not limited by pharmacopoeias accounted for more than 99.7 % of the number of micro-particles. In addition, the limits of insoluble nano-particles are not specified in pharmacopoeias. As NTA can accurately be used to determine the size and concentration of PS nano-spheres [39], NTA was also applied to determine the size and quantity of nano-scale insoluble particles in chemical injections for the first time in this study (Fig. 7). The sizes of these particles were in the range of 20–900 nm, and the concentration was from $6 \times 10^4$ to $1 \times 10^7$ p/mL, which was significantly higher than that of insoluble micro-particles.

### 4.3. Evaluation of the MNP particle identification and quantification by Py-GC/MS

Because of the defects that μRaman spectroscopy can only collect the apparent information of particles, and SEM-EDS only collects the element information of particles except hydrogen, theresults of μRaman and SEM-EDS determinations were further reviewed by Py-GC/MS. Although the size of the particles can't be identified by Py-GC/MS, the particle macromolecules can be cleaved into fragment ions, and characteristic ions $m/z$ 70, 83, and 126 were used to identify the signature product 2,4 dimethyl-1-heptene of PP [40]. The antioxidants, unpolymerized monomers, and other adsorbed chemicals were cracked off during the thermal desorption (300 °C) [25]. Since GF-B film and inorganic alumina film can withstand high temperature of 600 °C, the polymer can become fragment ions in the subsequent lysis stage. The particles on films enriched from injections were matched to ethylene-propylene copolymer P(E-P) or PP in the polymer library (Fig. 3). They might have come from bottles made of modified PP materials.

In terms of MNP quantification, the lysis ions of characteristic products are $m/z$ 69, 89, 100 in PMMA, 51, 78, 103, 104 in PS, 83, 97, 111, 140 in PE, and 135, 163, 194 in PET, respectively [41], owing to 70 in PP is close to 69 in PMMA, 83 is also present in PE, while $m/z$ 126 is only present in PP, so which is determined to be a quantitative ion. If 70 is used as the quantitative ion, the presence of PE will cause false positive interference in the determination of PP in tea [40]. Besides, because PP can't be dissolved and uniformly dispersed in water, according to the similar polarity of water and ethanol, the ethanol solvent was used as a dispersant, and the standard MNPs can be dispersed by stirring or ultrasonic, so as to ensure the successful completion of the standard curve and recovery experiments. Finally, the established assay had a LOQ for 10 ng (10-fold S/N), which was more sensitive than the Py-GC/MS method for the determination of MNP particles in blood for 50 ng [25]. Quantitative analysis was performed on identification results (Fig. 4), which were not found in the blank lysis cup, filter membrane, ultra-clean table bottom membrane and filtered water membrane. After dividing by the recovery rate (Table 2), the average concentrations of MP and NP particles were 34 and 23 μg/L, respectively. These values were lower than the 210 μg/L detected in the injections after UV irradiation for 6 weeks [11]. These results demonstrate that MNPs can be produced under improper storage conditions, not only because of indoor sunlight but also as a result of mechanical stress [34]. Based on the current per capita infusion volume of 10.4 bottles/year in China, it is estimated that the annual MP and NP particle quantity imported into the human body is 36 and 24 μg, respectively. In addition, although MNPs ($<$10 μm) in injections can enter the blood circulation through intravenous injection, their concentrations are much lower than those in the blood of healthy people (1.6 μg/mL). Thus, MNPs may presumably enter the body through inhalation, ingestion and skin contact [25]. Therefore, do they accumulate in the body?

### 4.4. MNP particles introduced into the body after infusion therapy partially accumulated in the body

It is remarkable that people have been injecting drugs intravenously for so many years. However, MNPs have not directly caused significant diseases. Are they mostly accumulated or excreted after administration? Radiation imaging experiments have revealed that PET-MNPs (1 μm, 35 μg) accumulated primarily in the liver and spleen of mice 168 h after intravenous injection, with a ratio of 60 %

and 15 %, respectively, and a ratio of 10 % were excreted in urine [12]. Similarly, after intravenous injection of PS nano-particles for 4 h, it was found that PS-NPs (100 nm, 80 μg) accumulated in the liver, spleen and lung of mice, and there was still no significant excretion at 28 days [42]. With the flow of blood, MPs such as PE, PP and PS appear in the pericardia, epicardial adipose, pericardial adipose, myocardia, left atrial appendages of human cardiac tissues (maximum 469 μm) and in the blood before and after surgery (maximum 184 μm), suggesting that accumulation may have occurred [43]. Furthermore, PP-MPs at 2–12 μm could enter the mammary gland through capillary walls and appear in the breast milk of lactating women with a concentration of 0.7 p/g [44]. Moreover, PP-MPs (4–15 μm) might be secreted into the tubule lumen after uptake from capillaries through the proximal glomerular tubule epithelial cells and then excreted into the urine of each healthy person at a quantity of 1 particle [45]. Finally, some PP-MPs in the size range of 2–6 μm may break through the 'blood–testis barrier', and enter the semen of a healthy man with a quantity of 1.6 particles [46]. In summary, the excreted particles were very small, only about 1 particle in average. Therefore, among the accumulated MNPs of 60 μg from the annual injection dose, most of the particles may be accumulated through the blood flowing to various tissues in the body.

### *4.5. Pathogenicity for the accumulation of MNP in the human body*

So whether the accumulated MNPs cause disease? Surprisingly, during the follow-up monitoring of 257 patients accumulated with PE (21.7 μg/g), PVC (5.2 μg/g) and other NP particles (<200 nm) in carotid plaque tissue, it was shown that the combined risk of myocardial infarction, stroke and death from any other reason is 4.53 times higher than not detected in tissue of patients [47], becoming a direct proof for NP particles cause disease. Because the selected population is not representative of the general population, the results cannot be generalized. Therefore, larger and more representative samples are needed to confirm the pathogenicity of MNPs.

Therefore, since infusion therapy can lead to the accumulation of MNPs in almost the tissues and organs of the whole body, it is recommended that people avoid or reduce infusion therapy. In addition, we should try to avoid extrusion and reduce the number of shaking in the transporting process of injections to reduce the release of plastic particles. Finally, it is recommended to place the container in a cool and dry place to avoid direct sunlight. The disadvantage of this study is that the alumina film is brittle and fragile, which can easily lead to the loss of NP particles when they are trapped weighed, and transferred to the lysis cup, which may be one of the reasons why the detection rate of NP is lower than that of MP particles. Second, there may be some defects in the identification of NP particles because EDS cannot detect hydrogen elements. It is hoped that more advanced technologies such as SEM-Raman or stimulated Raman spectroscopy can be used for accurate characterisation in the future to more accurately identify NPs and obtain accurate sizes.

## 5. Conclusion

In this study, we found for the first time that MNP particles such as P(E–P) and PP existed in commonly used PP-bottled injections with concentrations ranging from approximately 1 to 60 μg/L. The number of NP particles was more than 100 times that of MPs, and the proportions of MPs and NPs in the total number of particles in the solution were estimated to be 2.8 % and 18.1 %, respectively, indicating that the proportion of NPs was higher than that of MPs. In consideration of the regulatory particularity of injections by the national pharmacopoeia, the size of MPs was mainly 2–10 μm, and the size of NPs was mainly fragments or particles smaller than 50 nm. The size and concentration of MPs in the injections measured in this study filled the gap in the literature regarding insoluble MNP particles existing in the plastic-bottled injections within the validity period. This study also provides a foundation for further research into the toxicological effects of injections in mice and zebrafish.

## Data availability statement

The data included in article and supplementary material in article.

## Funding

The authors declare that this manuscript is supported by the Standard Substances and Standardization Management Center of National Institutes for Food and Drug Control [grant number 1080050090101], and the Project of Academic Leader Training Fund of National Institutes for Food and Drug Control [grant number 2023X9].

## CRediT authorship contribution statement

**Jie Wang:** Writing – original draft, Methodology, Data curation, Conceptualization. **Lan-Gui Xie:** Writing – review & editing, Methodology, Funding acquisition, Conceptualization. **Xian-Fu Wu:** Resources. **Zong-Ge Zhao:** Supervision. **Hui-Ying Yang:** Funding acquisition. **Hui-Min Sun:** Writing – review & editing, Supervision, Project administration, Conceptualization.

## Declaration of competing interest

The authors declare that they have no known competing *fi*nancial interests or personal relationships that could have appeared to in*fl*uence the work reported in this paper.

## Appendix A. Supplementary data

Supplementary data to this article can be found online at https://doi.org/10.1016/j.heliyon.2024.e35101.

## References


[1] C. Wang, C. Liu, L. Wan, A. Liao, J. An, Y. Luo, Research progress of infusion therapy in China, Chin. J. Mod. Nurs. 28 (2022) 3207–3215.
[2] Zhang W.F., Ma Y., Wang B., Bao W.J., Zhang L.Z., The invention relates to modified polypropylene soft bottle material, preparation method and application, Chinese Patient No. 104086905A. 12 (2014) 1-9.
[3] Y. Ruan, Y. Ding, Y. Lv, X. Chen, Z. Chen, M. Wang, The invention relates to a production process of sodium chloride injection in plastic bottle, Chinese Patient No. 105168127 A 12 (2015) 1–4.
[4] H. Wang, Analysis on reasons and control strategies of insoluble particles in chemical injections, Drug. Eva. Res. 45 (2022) 1909–1913.
[5] C.Y. Zhu, H.Y. Zuo, H.L. Li, R.S. Tong, Drug compatibility with various closed intravenous infusion containers, Front. Pharmacol. 14 (2024) 1265945.
[6] L. Wang, L. Yuan, H. Jiang, W. Yan, H.R. Cintrón-Colón, V.L. Perez, D.C. DeBuc, W.J. Feuer, J. Wang, Vessel sampling and blood flow velocity distribution with vessel diameter for characterizing the human bulbar conjunctival microvasculature. Eye. Contact, Lens. 42 (2016) (2016) 135–140.
[7] N.K. Prasad, R. Shome, G. Biswas, S.S. Ghosh, A. Dalal, Transport behavior of commercial anticancer drugprotein-bound paclitaxel (Paclicad) in a micron-sized channel, Langmuir 38 (2022) 2014–2025.
[8] Chinese Pharmacopoeia Commission, Beijing, China, China Medical Science and Technology Press, 2020, p. 125. Chinese pharmacopeia, part IV, (chapter 0903).
[9] The United States Pharmacopoeia Convention, Washington, USP, United States Pharmacopeia Press. United States Pharmacopeia, Part NF38, 2020, pp. 12–20 (chapter 1790).
[10] European Pharmacopoeia Commission, Strasbourg, France, European Directorate for the Quality of Medicines and Healthcare Press, European Pharmacopeia, 2020, p. 382 (chapter 2).9.19.
[11] X. Zhang, K. Shi, Y. Liu, Y. Chen, K. Yu, Y. Wang, H. Zhang, J. Jiang, Rapid and efficient method for assessing nanoplastics by an electromagnetic heating pyrolysis mass spectrometry, J. Hazard Mater. 419 (2021) 126506.
[12] S. Delaney, C. Rodriguez, S.M. Sarrett, E.J. Dayts, B.M. Zeglis, O. Keinänen, Unraveling the in vivo fate of inhaled micro- and nanoplastics with PET imaging, Sci. Total Environ. 904 (2023) 166320.
[13] R. Jia, J. Han, X. Liu, K. Li, W. Lai, L. Bian, J. Yan, Z. Xi, Exposure to polypropylene microplastics via oral ingestion induces colonic apoptosis and intestinal barrier damage through oxidative stress and inflammation in mice, Toxics 11 (2023) (2023) 127.
[14] J.H. Woo, H.J. Seo, J.Y. Lee, I. Lee, K. Jeon, B. Kim, K. Lee, Polypropylene nanoplastic exposure leads to lung inflammation through p38-mediated NF-κB pathway due to mitochondrial damage, Part. Fibre Toxicol. 20 (2023) 2.
[15] H.-S. Lee, D. Amarakoon, C.-i Wei, K.Y. Choi, D. Smolensky, S.-H. Lee, Adverse effect of polystyrene microplastics (PS-MPs) on tube formation and viability of human umbilical vein endothelial cells, Food Chem. Toxicol. 154 (2021) 112356.
[16] D.K. Sarma, R. Dubey, R.M. Samarth, S. Shubham, P. Chowdhury, M. Kumawat, V. Verma, R.R. Tiwari, M. Kumar, The biological effects of polystyrene nanoplastics on human peripheral blood lymphocytes, Nanomaterials 12 (2022) 1632.
[17] S. Lin, H. Zhang, C. Wang, X.-L. Su, Y. Song, P. Wu, Z. Yang, M.-H. Wong, Z. Cai, C. Zheng, Metabolomics reveal nanoplastic-induced mitochondrial damage in human liver and lung cells, Environ. Sci. Technol. 56 (2022) 12483–12493.
[18] J. Hu, Y. Zhu, J. Zhang, Y. Xu, J. Wu, W. Zeng, Y. Lin, X. Liu, The potential toxicity of polystyrene nanoplastics to human trophoblasts in vitro, Environ. Pollut. 311 (2022) 119924.
[19] V. Kopatz, K. Wen, T. Kovács, A.S. Keimowitz, V. Pichler, J. Widder, A.D. Vethaak, O. Hollóczki, L. Kenner, Micro- and nanoplastics breach the blood–brain barrier (BBB): biomolecular corona's role revealed, Nanomaterials 13 (2023) 1404.
[20] X. Wu, P. Liu, H. Huang, S. Gao, Adsorption of triclosan onto different aged polypropylene microplastics: critical effect of cations, Sci. Total Environ. 717 (2020) 137033.
[21] R.M. Razanajatovo, J. Ding, S. Zhang, H. Jiang, H. Zou, Sorption and desorption of selected pharmaceuticals by polyethylene microplastics, Mar. Pollut. Bull. 136 (2018) 516–523.
[22] X. Liu, J. Xu, Y. Zhao, H. Shi, C.H. Huang, Hydrophobic sorption behaviors of 17β-Estradiol on environmental microplastics, Chemosphere 226 (2019) 726–735.
[23] P.M. Gopinath, V. Saranya, S. Vijayakumar, M. Mythili Meera, S. Ruprekha, R. Kunal, A. Pranay, J. Thomas, A. Mukherjee, N. Chandrasekaran, Assessment on interactive prospectives of nanoplastics with plasma proteins and the toxicological impacts of virgin, coronated and environmentally released-nanoplastics, Sci. Rep. 9 (2019) 8860.
[24] K. Munno, H. De Frond, B. O'Donnell, C.M. Rochman, Increasing the accessibility for characterizing microplastics: introducing new application-based and spectral libraries of plastic particles (SLoPP and SLoPP-E), Anal. Chem. 92 (2020) 2443–2451.
[25] H.A. Leslie, M.J. Van Velzen, S.H. Brandsma, A.D. Vethaak, J.J. Garcia-Vallejo, M.H. Lamoree, Discovery and quantification of plastic particle pollution in human blood, Environ. Int. 163 (2022) 107199.
[26] The International Council for Harmonisation of Technical Requirements for Pharmaceuticals for Human Use, Governing Principle of Validation of Analytical Procedures: Text and Methodology, Q2, 2005. R1).
[27] J.C. Prata, A. Paço, V. Reis, J.P. da Costa, A.J.S. Fernandes, F.M. da Costa, A.C. Duarte, T. Rocha-Santos, Identification of microplastics in white wines capped with polyethylene stoppers using micro-Raman spectroscopy, Food Chem. 331 (2020) 127323.
[28] L. Zhu, M. Ma, H. Wu, L. An, Z. Yang, Occurrence of microplastics in commercially sold bottled water, Sci. Total Environ. 867 (2023) 161553.
[29] V. Shruti, F. Pérez-Guevara, G. Kutralam-Muniasamy, Metro station free drinking water fountain-A potential "microplastics hotspot" for human consumption, Environ. Pollut. 261 (2020) 114227.
[30] P.A. Da Costa Filho, D. Andrey, B. Eriksen, R.P. Peixoto, B.M. Carreres, M.E. Ambühl, J.B. Descarrega, S. Dubascoux, A. Panchaud, Detection and characterization of small-sized microplastics (≥ 5 μm) in milk products, Sci. Rep. 11 (2021) 1–13.
[31] Y. Li, L. Peng, J. Fu, X. Dai, G. Wang, A microscopic survey on microplastics in beverages: the case of beer, mineral water and tea, Analyst 147 (2022) 1099–1105.
[32] T. Yang, J. Luo, B. Nowack, Characterization of nanoplastics, fibrils, and microplastics released during washing and abrasion of polyester textiles, Environ. Sci. Technol. 55 (2021) 15873–15881.
[33] E. Fries, J.H. Dekiff, J. Willmeyer, M.T. Nuelle, M. Ebert, D. Remy, Identification of polymer types and additives in marine microplastic particles using pyrolysis-GC/MS and scanning electron microscopy, Environ. Sci. Process. Impacts. 15 (2013) 1949–1956.
[34] A. Winkler, N. Santo, M.A. Ortenzi, E. Bolzoni, R. Bacchetta, P. Tremolada, Does mechanical stress cause microplastic release from plastic water bottles? Water Res. 166 (2019) 115082.
[35] N. Qian, X. Gao, X. Lang, H. Deng, T.M. Bratu, Q. Chen, P. Stapleton, B. Yan, W. Min, Rapid single-particle chemical imaging of nanoplastics by SRS microscopy, Proc. Natl. Acad. Sci. U. S. A. 121 (2024) e2300582121.
[36] J. Weisser, I. Beer, B. Hufnagl, T. Hofmann, H. Lohninger, N.P. Ivleva, K. Glas, From the well to the bottle: identifying sources of microplastics in mineral water, Water 13 (2021) 841.

[37] Y. Huang, K.K. Wong, W. Li, H. Zhao, T. Wang, S. Stanescu, S. Boult, B. van Dongen, P. Mativenga, L. Li, Characteristics of nano-plastics in bottled drinking water, J. Hazard Mater. 424 (Pt C) (2022) 127404.
[38] Z.R. Ayala, S. Judge, S. Angl′es, D.I. Greenfield, A comparison between the FlowCam 8100, microscopy, and sandwich hybridization assay for quantifying abundances of the saxitoxin-producing dinoflagellate, Alexandrium catenella, Harmful Algae 125 (2023) 102423.
[39] M. Tong, O.S. Brown, P.R. Stone, L.M. Cree, L.W. Chamley, Flow speed alters the apparent size and concentration of particles measured using NanoSight nanoparticle tracking analysis, Placenta 38 (2016) 29–32.
[40] Z. Yue, X. Liu, T. Mei, Y. Zhang, F. Pi, H. Dai, Y. Zhou, J. Wang, Reducing microplastics in tea infusions released from filter bags by pre-washing method: quantitative evidences based on Raman imaging and Py-GC/MS, Food Chem. 445 (2024) 138740.
[41] L.F. Amato-Lourenço, R. Carvalho-Oliveira, G.R. Júnior, L. Dos Santos Galvão, R.A. Ando, T. Mauad, Presence of airborne microplastics in human lung tissue, J. Hazard Mater. 416 (2021) 126124.
[42] X. Zhao, Y. Wang, Y. Ji, R. Mei, Y. Chen, Z. Zhang, X. Wang, L. Chen, Polystyrene nanoplastics demonstrate high structural stability in vivo: a comparative study with silica nanoparticles via SERS tag labeling, Chemosphere 300 (2022) 134567.
[43] Y. Yang, E. Xie, Z. Du, Z. Peng, Z. Han, L. Li, R. Zhao, Y. Qin, M. Xue, F. Li, K. Hua, X. Yang, Detection of various microplastics in patients undergoing cardiac surgery, Environ. Sci. Technol. 57 (2023) 10911–10918.
[44] A. Ragusa, V. Notarstefano, A. Svelato, A. Belloni, G. Gioacchini, C. Blondeel, E. Zucchelli, C. De Luca, S. D'Avino, A. Gulotta, Raman microspectroscopy detection and characterisation of microplastics in human breastmilk, Polymers 14 (2022) 2700.
[45] C. Pironti, V. Notarstefano, M. Ricciardi, O. Motta, E. Giorgini, L. Montano, First evidence of microplastics in human urine, a preliminary study of intake in the human body, Toxics 11 (2022) 40.
[46] L. Montano, E. Giorgini, V. Notarstefano, T. Notari, M. Ricciardi, M. Piscopo, O. Motta, Raman Microspectroscopy evidence of microplastics in human semen, Sci. Total Environ. 901 (2023) 165922.
[47] R. Marfella, F. Prattichizzo, C. Sardu, G. Fulgenzi, L. Graciotti, T. Spadoni, N. D'Onofrio, L. Scisciola, R. La Grotta, C. Frigé, V. Pellegrini, M. Municinò, M. Siniscalchi, F. Spinetti, G. Vigliotti, C. Vecchione, A. Carrizzo, G. Accarino, A. Squillante, G. Spaziano, D. Mirra, R. Esposito, S. Altieri, G. Falco, A. Fenti, S. Galoppo, S. Canzano, F.C. Sasso, G. Matacchione, F. Olivieri, F. Ferraraccio, I. Panarese, P. Paolisso, E. Barbato, C. Lubritto, M.L. Balestrieri, C. Mauro, A. E. Caballero, S. Rajagopalan, A. Ceriello, B. D'Agostino, P. Iovino, G. Paolisso, Microplastics and nanoplastics in atheromas and cardiovascular events, N. Engl. J. Med. 390 (2024) 900–910.